A major purpose of the Techni- Information Center is to provide broadest dissemination possi- of information contained in)E's Research and Development ports to business, industry, the ademic community, and federal, ıte and local governments.

Although a small portion of this)ort is not reproducible, it is ng made available to expedite availability of information on the search discussed herein.

LA-UR -84-1199
CONF

NOTICE

PORTIONS OF THIS REPORT ARE ILLEGIBLE. It has been reproduced from the best available copy to permit the broadest possible availability.

Los Alamos National Laboratory is operated by the University of California for the United States Department of Energy under contract W-7405-ENG-36.

CONF-840256--3

TITLE: ELECTRON VELOCITY DISTRIBUTIONS NEAR COLLISIONLESS SHOCKS

LA-UR--84-1199

DE84 011352

AUTHOR(S): William C. Feldman

SUBMITTED TO: Proceedings of Napa Valley Shock Conference, 20-24 February 1984, Napa Valley, CA

DISCLAIMER

MASTER

Los Alamos Los Alamos National Laboratory
Los Alamos, New Mexico 87545

FORM NO 836 R4

Electron Velocity Distributions Near Collisionless Shocks

William C. Feldman

Los Alamos National Laboratory

Los Alamos, NM 87545

ABSTRACT

Recent studies of the amount of electron heating and of the shapes of electron velocity distributions across shocks near the earth are reviewed. It is found that electron heating increases with increasing shock strength but is always less than the ion heating. The scale length of electron heating is also less than that for the ions. Electron velocity distributions show characteristic shapes which depend on the strength of the shocks. At the weaker shocks, electron heating is mostly perpendicular to the ambient magnetic field, $\bar{B}$, and results in Gaussian-shaped velocity distributions at low-to-moderate energies. At the stronger shocks, parallel heating predominates resulting in flat-topped velocity distributions. A reasonable interpretation of these results indicates that at the weaker shocks electron heating is dominated by a tendency toward conservation of the magnetic moment. At the stronger fast-mode shocks, this heating is thought to be dominated by an acceleration parallel to $\bar{B}$ produced by the macroscopic shock electric field followed by beam driven plasma instabilities. Some contribution to the heating at the stronger shocks from conservation of the magnetic moment and cross-field current-driven instabilities cannot be ruled out. Although the heating at slow mode shocks is also dominated by instabilities driven by magnetic field-aligned electron beams, their acceleration mechanism is not yet established.

I. Introduction

Collisionless shocks are a ubiquitous structure present in astrophysical plasmas. They form naturally from the steepening of pressure waves generated by temporal and/or spatial perturbations induced in both the interplanetary and interstellar plasmas. Although their gross structure is determined by the macroscopic conservation laws, their internal structure depends importantly on details of the microscopic dissipation mechanisms necessitated by the gross structure. This internal structure is in turn important since it regulates the flow of energy from the steepened wave to other channels which affect the ambient medium on a global scale. The amount of electron heating as well as the detailed shapes of electron velocity distributions near collisionless shocks are a very sensitive probe of this internal structure because the energy density of the shock-associated electric and magnetic fields is generally large compared to the energy density of the upstream electron population.

The purpose of this paper is to review present knowledge of electron heating at collisionless shocks in near-earth plasmas. It is organized into two distinct sections; the amount of heating when electrons are viewed as a fluid (section 2), and the heating mechanism as determined from measured shapes of electron velocity distributions (section 3). Section 4 provides a summary and conclusion.

From the fluid viewpoint, in situ measurements made over the past two decades have shown the magnitude of electron heating to increase with increasing shock strength but to be generally less than the magnitude of ion heating. Electrons are also observed to heat over a length scale shorter than

that over which the ions heat. From the microscopic viewpoint, shapes of electron velocity distributions across many shocks near the earth show that the mechanism of heating depends on shock strength. At the weaker shocks most of the observed heating is consistent with a tendency to conserve the magnetic moment. In contrast, at the stronger shocks, electron heating is generally thought to be dominated by an acceleration parallel to the magnetic field, $\bar{B}$, followed by beam-driven plasma instabilities.

2. Fluid Electron Heating

Conservation of mass, momentum and energy requires the heating of a plasma upon passage from the upstream to downstream sides of a shock (see e.g. Tidman and Krall, 1971). The same conservation laws require the ratio of downstream to upstream temperatures, T(d/u), to increase with increasing shock strength. Another parameter which should increase monotonically with increasing shock strength is the ratio of downstream to upstream densities, N(d/u). Because of these facts, various theoretical applications of the resultant shock-jump conditions (as approximated by the Rankine-Hugoniot relations) to general astrophysical situations have replaced the energy conservation equation by a simple polytrope law, $T(d/u) = N(d/u)^{\gamma-1}$ to simplify the calculations. According to thermodynamics, if the transition is adiabatic, γ is the ratio of specific heats and therefore provides a measure of the number of degrees of freedom which participate in the compression. However, a necessary limitation of all fluid theories is that none can predict the partition of the resultant heating between electron and ion components of the plasma. Such partition depends on a variety of microprocesses requiring a nonlinear, kinetic description of gas.

It has long been known that collisionless shocks do not heat electrons as efficiently a they heat ions (Montgomery et al. 1970; Hundhausen et al., 1970; Hundhausen, 1970a,b). An example which illustrates this fact for measurements across both the earth's bow shock and an interplanetary shock on 26 Feb., 1969 is shown in Figure 1 (Hundhausen et al., 1970). Whereas the ratios of downstream to upstream electron temperatures are $T_e(d/u) \tilde{=} 2.8$ and 1.1 for the bow shock and interplanetary shocks, respectively, those for the proton temperatures are $T_p\ (d/u) \tilde{=} 50$ and 3.3, respectively. These ratios are fairly representative of average conditions. Electron temperature ratios across the bow shock have been observed to range between 1.25 and 9.5 with an average of about 3.0 (Montgomery et al., 1970; Scudder et al., 1973; Bame et al., 1979; Ogilvie and Scudder, 1979). The same ratio across interplanetary shocks range between 1.0 and 3.0 with an average of 1.5 (Feldman et al., 1983b).

The dependence of electron and proton heating on shock strength is illustrated in figure 2 for a sample of 41 interplanetary shocks (Feldman et al., 1983b). Superimposed are straight lines representing polytrope relations having adiabatic compressions in 1, 2 and 3 dimensions. Although both electron and ion heating increases with increasing shock strength, none of the polytrope relations provide an adequate representation of all the data. This observation, however, does not rule out the possibility that individual shock transitions obey differing polytrope relations.

The relative efficiency for heating electrons and ions across the same sample of interplanetary shocks is illustrated in figure 3 (Feldman et al., 1983b). The straight line represents equal heating, $T_e(d/u) = T_p(d/u)$. Inspection shows that the ratio, $T_p(d/u)/T_e(d/u)$ is always greater than 1 and

generally increases with increased heating and hence from figure 2, increased shock strength as indicated by N(d/u).

Another fact which indicates the microscopic complexity of electron and ion heating across collisionless shocks is their differing length scales. Whereas electrons generally heat rapidly near the upstream edge of the shock the ions heat over a much broader region extending well into the downstream region (Montgomery et al., 1970; Montgomery, 1970; Bame et al., 1979; Goodrich, 1984; Quest, 1984). An example illustrating this fact for a bow shock crossing on 7 November 1977 is shown in figure 4 (Bame et al., 1979). Comparison of the width of the wedge giving the length scale for proton heating, with the trace of electron temperature underneath for the same shock crossed by ISEE 1 (above) and ISEE 2 (below), demonstrates this point.

A more explicit illustration of the differing length scales of electron and proton heating is shown in figures 5 and 6, respectively, for a bow shock crossing on 5 June 1967 (Montgomery, 1970). The numbered spectra in each figure correspond to nearly simultaneous locations which increase in penetration depth from the upstream (1) to the downstream (3) plasma regions. Comparison of the intermediate spectra (2) in each figure with those representing upstream (1) and downstream (3) conditions shows that whereas the proton spectrum shows a higher energy, low-flux component superimposed on a decelerated yet still cold main solar wind beam, the electrons have already heated to their final downstream state.

3) Electron Heating Mechanism

A shock transition is, by definition, a relatively thin surface across which the upstream plasma suffers an irreversible change in state upon passage to the downstream region. This irreversibility, in turn, requires some form of microscopic dissipation. A self-consistent, two-step process is usually envisaged. Macroscopic electric and magnetic fields are generated within the shock layer in order to conserve mass, momentum and energy. These fields induce adiabatic changes in particle velocity distributions raising their level of free energy. Beyond levels which depend on the nature of the free energy and the ambient plasma conditions, waves can be driven unstable leading to irreversible dissipation. This dissipation not only reduces the free energy below its respective threshold level but also affects the mass, momentum and energy balance across the shock. The shock-associated macroscopic fields must then adjust to achieve self-consistency.

Applications to electrons have concentrated on three types of free energy (see e.g. Tidman and Krall, 1971; Forslund and Shonk, 1970; Winske, 1984): 1) Changes in the magnetic field, $\bar{B}$, across shocks induce a current, $\bar{J} = \frac{C}{4\pi}(\bar{\nabla}x\bar{B})$, carried almost entirely by the electrons. Enhanced free energy then results from the electron-ion relative drift speed, $V_D = J/(Ne)$, where N is the number density and e is the electronic charge. 2) Changes in the magnitude of $\bar{B}$ cause anisotropies in electron velocity distributions through conservation of the magnetic moment, $\mu \propto T_\perp/B$, where $T_\perp$ is the component of temperature perpendicular to $\bar{B}$. This effect will tend to increase $T_\perp$ across fast-mode shocks and decrease $T_\perp$ across slow-mode shocks. 3) Changes in the

macroscopic electrostatic potential, Φ, can accelerate electrons parallel to $\bar{B}$ thereby enhancing the parallel free energy.

Each of the foregoing free energy sources and their consequent microscopic dissipation processes (see e.g. review by Winske, 1984) impart a characteristic distortion to ambient electron velocity distributions. Assuming these distributions have Gaussian shapes initially in the upstream region, 1) an induced current will appear within the transition layer as an offset Gaussian having drift velocity parallel to the shock surface, 2) conservation of μ will appear downstream of fast-mode (slow-mode) shocks as a Gaussian with increased (decreased) $T_\perp$, and upstream of fast-mode shocks as a Gaussian having a superimposed mirrored population, and 3) acceleration parallel to $\bar{B}$ will appear downstream as a beam with drift velocity parallel to $\bar{B}$. The occurrence of dissipation at the shock will appear upstream (downstream) as an upstream (downstream) directed heat flux.

We start first with a review of observations across low-Mach number, fast-mode shocks. A recent survey of electron velocity distributions, F(v), near interplanetary shocks which often satisfy this criterion, showed heating mainly perpendicular to $\bar{B}$ (Feldman et al., 1983c). This effect is demonstrated in figure 7 for 3 low-Mach number, interplanetary shocks by overlays of cuts through upstream and downstream velocity distributions aligned parallel (left-hand panel) and perpendicular (right-hand panel) to $\bar{B}$, respectively. Whereas little difference is seen between upstream and downstream $F(v_\parallel)$ in the left-hand panel, the downstream $F(v_\perp)$ is definitely broader than the upstream $F(v_\perp)$ in the right-hand panel. In spite of this heating, however, the shapes of both upstream and downstream $F(v_\perp)$ are very similar. Both of these

qualitative effects are expected if the heating results from conservation of the magnetic moment, μ. A quantitative confirmation of this mechanism is demonstrated in figure 8 for another interplanetary shock. This shock was stronger than the other three. As a result, some parallel heating is seen in the left-hand panel. However inspection of the upstream (triangles) and downstream (squares) perpendicular cuts overlayed in the right-hand panel shows that the perpendicular heating is larger. Also included in the right-hand panel is the perpendicular cut through F(v) (circles) generated from that measured upstream assuming $\mu = v_\perp^2/B$ = constant. Comparison with the $F(v_\perp)$ measured downstream shows that conservation of μ provides a close fit to the measured $F(v_\perp)$ at low energies but overestimates the heating at high energies. Since the low-energy part of $F(v_\perp)$ contains most of the electrons, the predicted and measured values of $T_\perp$ are nearly equal.

Heating parallel to $\bar{B}$ becomes relatively more important for the stronger, fast-mode shocks. The shapes of downstream velocity distributions also change with shock strength. Whereas at low N(d/u) the shapes are Gaussian at low energies as shown in figure 7, at high N(d/u) they have flat tops at low energies (Montgomery et al., 1970; Scudder et al., 1973; Ogilvie and Scudder, 1979; Feldman et al., 1982b). Figure 9 shows the first published example of a flat-topped electron velocity distribution measured just downstream of the earth's bow shock (Montgomery et al., 1970). Figure 10 shows overlayed parallel and perpendicular cuts through distributions measured just downstream of two relatively strong interplanetary shocks demonstrating the generally greater importance of parallel heating (Feldman et al., 1983c). Similar distributions measured downstream of a set of interplanetary shocks having strengths which spanned the range $1 < N(d/u) < 4$, were fit with modified

Gaussian functions of the form $f_G(v) = A_{exp}[-X^S]$, where $X = (v-v_A)/v_o$. This form has the virtue that it is Gaussian when S=2 but becomes increasingly flat for $v < v_A$ as S increases above 2. The results of this analysis are summarized in figures 11 and 12 (Feldman et al., 1983c). They show that downstream distributions become increasingly flat as the shock strength increases and that electron heating increases with increasing flatness.

Details of possible electron heating mechanisms have come from studies of the earth's bow shock because it stands in the solar wind flow and can therefore be probed with higher spatial resolution. The first indication of nonreversible electron heating came from observations of a separate component of suprathermal electrons upstream of the shock (Scarf et al., 1971; Fredericks et al., 1971; Neugebauer et al., 1971). The first attempt at a quantitative measure of the energy flux transported by these electrons posed difficulties in interpretation because it showed a substantial flux carried by electrons having energy above 10 keV yet the amount carried below 10 keV was already greater than that carried on average by the total (mostly convective) solar wind (Ogilvie et al., 1971). However subsequent measurements have shown that both the average backstreaming energy flux (Feldman et al., 1973) and the downstreaming energy flux (Ogilvie and Scudder, 1979) are of order 10^{-2} ergs cm^{-2} s^{-1}, representing a significant energy loss to the plasma within the shock transition layer. Whereas the downstreaming heat flux has been observed throughout the magnetosheath (Reiff and Reasoner, 1975; Ogilvie and Scudder, 1979), the backstreaming heat flux has been observed as far upstream as the moon (~60 earth radii, R_e, Reasoner, 1975) and the inner sun-earth Lagrangian point (~266 R_e, Feldman et al., 1982a).

Insight into the dominant electron heating mechanism operating within the earth's bow shock has come from measurements made using the ISEE 1/2 fast plasma analyzer (Bame et al., 1979). Cuts through 2-D velocity distributions parallel to $\bar{B}$ show the formation of a downstream-directed electron beam superimposed on a flat-topped background component as shown in figure 13 (Feldman et al., 1982b; Feldman et al., 1983a). Inspection of this example, as well as of many others, shows that the maximum of $F(v_{\parallel})$ in the beam decreases as its mean energy increases with increasing penetration into the shock from its upstream edge. Eventually the part of $F(v_{\parallel})$ representing the beam, merges into the nearly flat-topped or slightly concave upward (see e.g. figure 5) shaped distributions characteristic of the downstream magnetosheath. Although the example in figure 13 represents the general case, one example of beams having directions which alternate within a quasi-perpendicular shock has been reported (Thomson et al., 1984). Because of the near perpendicular geometry it is not clear whether this example represents a separate phenomenon or just reflects beams entering the magnetosheath from both intersections of the interplanetary magnetic field line with the curved bow shock (see e.g. discussion in Feldman et al., 1983a).

These observations lend themselves to a simple interpretation. which is a small modification of that originally proposed by Forslund and Shonk (1970). Electron velocity distributions within the bow shock seem to be shaped by the interaction between the downstream-directed component of incident solar wind electrons, the upstream-directed component of magnetosheath electrons and the macroscopic, shock-associated electrostatic potential. A schematic picture of this interaction is given in figure 14. Here, representations of $F(v_{\parallel})$ are given at four different locations relative to the electrostatic potential ramp

assuming that microscopic processes are not operating. The distribution just upstream of the shock (position 1) is therefore composed of two halves separated by $v_{\parallel} = 0$. The electrons travelling to the right have not yet encountered the shock and therefore still carry the shape of ambient solar wind velocity distributions. Those travelling to the left are magnetosheath electrons which have been decelerated by the potential, Φ. In order to reach the upstream region, these electrons must have had initial kinetic energies in the magnetosheath, E_{ms}, sufficient to overcome $e\Phi_o$, the total potential drop. Their parallel energies in the solar wind are therefore $E_{\parallel} = E_{ms} - e\Phi_o$ with minimum $E_{\parallel} = 0$. Part way up the ramp within the shock transition layer (positions 2 and 3) electron distributions have three distinct parts. Electrons to the left of the dashed vertical lines labelled V_k with $k = 2, 3$ in figure 14, refer to unbound magnetosheath electrons having energies $E_{\parallel} = E_{ms} - e\Phi_k$. Their minimum energies are $E_{\parallel k} = \frac{1}{2} mV_k^2 = e\Phi_k$. Between the two vertical dashed lines corresponding to speeds between $\pm V_k$, are electrons trapped by the potential well bounding the magnetosheath along $\bar{B}$. Their velocity distribution is observed to be flat topped at low energies hence their representation as such in figure 14. To the right of the vertical dashed line at $-V_k$ are the initial solar wind electrons which have been accelerated through $e\Phi_k = \frac{1}{2} mV_k^2$ and thereby cooled. In the magnetosheath (panel 4) the distributions should be similar to those observed within the transition layer with the exception that there $\frac{1}{2} mV_4^2 = e\Phi_o$, the total potential drop. The similarities between the measured distributions in figure 13 and those pictured in figure 14 are evident. The differences, presumably, result from plasma instabilities generated by the accelerated solar wind beam. Theoretical analyses of measured distributions support this presumption (Thomsen et al., 1983; Tokar et al., 1984).

Electron velocity distributions similar to those shown in figure 13 have been observed across slow-mode shocks bounding the plasma sheet in the deep geomagnetic tail (Feldman et al., 1984). Examples representing parallel cuts through distributions measured 1) in the downstream plasma sheet (triangles), 2) within the shock transition layer (squares), and 3) in the upstream lobe (circles), at about 19:20 UT on 2 Feb. 1983, are shown in figure 15. The solid curve gives the Gaussian function providing a best fit to the 8 lowest energy points of the measured upstream (lobe) distribution. The difference between this curve and the measured distribution, outlined as the hatched region at negative electron speeds, identifies those electrons which carry the heat flux from the shock-heated transition layer into the upstream lobe.

Inspection of the distribution measured within the transition layer shows a beam at about $v_{\parallel}$ = +4200 km/s. This beam has a velocity of opposite sign to those of the electrons which carry the heat flux into the lobe. It is therefore directed into the downstream region, the same orientation as that observed at the earth's bow shock. The velocity distribution measured downstream of the shock in the plasma sheet is also seen to be very similar to typical magnetosheath distributions just downstream of the bow shock, both are nearly flat topped or slightly concave upward.

Because the similarities in measured velocity distributions are so close, it is reasonable to presume that the dominant heating mechanism within slow-mode shocks is the same as that inferred to heat electrons within strong, fast-mode shocks. In both, electrons are accelerated into the downstream region. The resultant downstream-directed beams are unstable to the generation of waves which then act to reduce the source of free energy by scattering and diffusing

the beam into a nearly flat-topped velocity distribution. A remnant of the original beam in the form of a slightly concave upward, downstream velocity distribution sometimes remains.

Much theoretical work on the physics of fast-mode shocks has shown that the force which accelerates electrons across these shocks into the downstream region is the component of the gradient in the macroscopic electrostatic potential which is parallel to B (Goodrich and Scudder, 1984). Because our understanding of slow-mode shock is much less complete, it is not known whether the same mechanism controls the downstream electron acceleration here as well. If this interpretation is correct then the electrostatic potentials across both fast- and slow-mode shocks have the same sign. Both then act to decelerate incident upstream ions and to accelerate incident upstream electrons. This fact is significant because the gradients in magnetic field are opposite across the two types of shocks. Whereas the resultant $\bar{J}x\bar{B}$ force acts to decelerate the plasma incident on fast-mode shocks, it acts to accelerate the plasma into slow-mode shocks. Although the electrostatic potential can act to balance this force in the electron momentum equation for fast-mode shocks, a potential of the same sign cannot provide the same balance across slow-mode shocks. Consequently, if the electron beams observed within slow shocks are accelerated by electric fields, then the $\bar{J}x\bar{B}$ force must act only on the ions. However it is also possible that the beams within slow shocks result from more complex macroscopic electric and magnetic fields so that both contribute to beam generation. Numerical simulations could possibly provide some answers to this question.

4) Summary and Conclusions

Information bearing on electron heating mechanisms operating at collisionless shocks in near-earth space has been reviewed. When considered as a fluid, electron heating increases with increasing shock strength but remains always less than the ion heating. The scale length of electron heating is also generally less than that of the protons. A consequence of this difference is that there usually exists a part of the shock-transition layer near the upstream edge within which the electron temperature is higher than the temperature of the main proton component.

The dominant mechanism which heats electrons depends on shock strength. At the weaker shocks electrons heat primarily perpendicular to $\bar{B}$ by conserving their magnetic moment. This mechanism transforms the usually Gaussian upstream velocity distributions into Gaussian-shaped downstream distributions. In contrast, electrons heat primarily parallel to $\bar{B}$ at the stronger shocks forming flat-topped downstream velocity distributions. The dominant mechanism responsible for this heating at fast-mode shocks is thought to be the acceleration of a magnetic field-aligned electron beam into the downstream region by the parallel component of a macroscopic electric field. Thermalization results from beam-driven microinstabilities. Although progress in understanding the relationship between electron heating and the cross-shock potential drop has been made recently (Goodrich and Scudder, 1984) many uncertainties remain. Possible contributions to the total heating from conservation of the magnetic moment and from cross-field, current-driven instabilities in these shocks cannot be ruled out.

Electron heating at slow-mode shocks is also dominated by the thermalization of downstream-directed electron beams. However for this case, the acceleration mechanism is not yet established. If the force causing the acceleration results from a macroscopic electric field, then the field must have the same sign as that within fast-mode shocks. In this case the $\bar{J}x\bar{B}$ force resulting from the magnetic field gradient must act only on the ions. However it is possible that both electrostatic potential and magnetic field gradients accelerate the observed electron beams in which case the shock structure must be more complex. It might be possible to resolve this question using numerical simulations.

Although much has been learned by past studies of electron heating at collisionless shocks, many questions remain unresolved. For example, it is not known what determines the magnitude of the electrostatic potential across fast-mode shocks and how it depends on the various plasma parameters such as 1) the upstream ratio of plasma to magnetic pressure, 2) the angle between the magnetic field and the shock normal, and 3) the upstream Mach number. Nor is it known what determines how much energy electrons can gain from the electrostatic potential upon crossing the shock. This energy is an important factor in the final partition of thermal energy between electrons and ions. The role of cross-field current-driven instabilities is also uncertain at the date of this review. And finally, the physics controlling electron heating at slow-mode shocks is completely unknown.

Acknowledgments

I have benefitted greatly from many discussions with M. Thomsen, J. Gosling, P. Gary, D. Forslund, K. Quest, K. Lee, and D. Winske. In this sense this review is really a collaborative effort although the name of only one author is placed beneath the title. This research was conducted under the auspices of the U.S. Department of Energy.

References

Bame, S. J., J. R. Asbridge, H. E. Felthauser, J. P. Glore, G. Paschmann, P. Hemmerich, K. Lehman, and H. Rosenbauer, ISEE-1 and ISEE-2 fast plasma experiment and the ISEE-1 solar wind experiment, IEEE Trans. Geosci. Electron., GE-16, 236, 1979.

Bame, S. J., J. R. Asbridge, J. T. Gosling, M. Halbig, G. Paschmann, N. Sckopke, and H. Rosenbauer, High temporal resolution observations of electron heating at the bow shock, Space Sci. Rev., 23, 75, 1979.

Feldman, W. C., J. R. Asbridge, S. J. Bame, and M. D. Montgomery, Solar wind heat transport in the vicinity of the earth's bow shock, J. Geophys. Res., 78, 3697, 1973.

Feldman, W. C., R. C. Anderson, J. R. Asbridge, S. J. Bame, J. T. Gosling and R. D. Zwickl, Plasma electron signature of magnetic connection to the earth's bow shock: ISEE 3, J. Geophys. Res., 87, 632, 1982a.

Feldman, W. C., S. J. Bame, S. P.Gary, J. T. Gosling, D. McComas, M. F. Thomsen, G. Paschmenn, N. Sckopke, M. M. Hoppe, and C. T. Russell, Electron heating within the earth's bow shock, Phys. Rev. Letters, 49, 199, 1982b.

Feldman, W. C., R. C. Anderson, S. J. Bame, S. P. Gary, J. T. Gosling, D. J. McComas, M. F. Thomsen, G. Paschmann, and M. M. Hoppe, Electron velocity distributions near the earth's bow shock, J. Geophys. Res., 88, 96, 1983a.

Feldman, W. C., J. R. Asbridge, S. J. Bame, J. T. Gosling, and R. D. Zwickl, Electron heating at interplanetary shocks in "Solar Wind 5," M. Neugebauer, ed., NASA Conf. Pub. 2280, p. 403, 1983b.

Feldman, W. C., R. C. Anderson, S. J. Bame, J. T. Gosling and R. D. Zwickl, Electron velocity distributions near interplanetary shocks, J. Geophys. Res., 88, 9949, 1983c.

Forslund, D. W., and C. R. Shonk, Formation and structure of electrostatic collisionless shocks, Phys. Rev. Lett., 25, 1699, 1970.

Fredericks, R. W., F. L. Scarf, and L. A. Frank, Nonthermal electrons and high frequency waves in the upstream solar wind 2. Analyses and interpretation, J. Geophys. Res., 76, 6691, 1971.

Goodrich, C., Numerical simulations of quasiperpendicular collisionless shocks, in "Proceedings of the Chapman Conf. on Collisionless Shock Waves in the Heliosphere," Napa Valley, California, 20-24 Feb., 1984.

Goodrich, C. C., and J. D. Scudder, The adiabatic energy change of plasma electrons and the frame dependence of the cross shock potential at collisionless magnetosonic shock waves, J. Geophys. Res., in press, 1984.

Hundhausen, A. J., Shock waves in the solar wind, in "Particles and Fields in the Magnetosphere," B. M. McCormac, ed., D. Reidel, Dordrecht-Holland, p.79, 1970a.

Hundhausen, A. J., Plasma measurements across the bow shock and in the magnetosheath, in "Intercorrelated Satellite Observations Related to Solar Events," V. Manno and D. E. Page, eds., D. Reidel, Dordrecht-Holland, p. 155, 1970b.

Hundhausen, A. J., S. J. Bame, and M. D.Montgomery, On observation of the Feb. 16, 1969 interplanetary shock wave, in "Intercorrelated Satellite Observations Related to Solar Events," V. Manno and D. E. Page, eds., D. Reidel, Dordrecht-Holland, p. 567, 1970.

Montgomery, M. D., Plasma measurements near the earth's bow shock: Vela 4, in "Particles and Fields in the Magnetosphere," B. M. McComac, ed., D. Reidel, Dordrecht-Holland, p. 95, 1970.

Montgomery, M. D., J. R. Asbridge, and S. J. Bame, Vela 4 plasma observations near the earth's bow shock, J. Geophys. Res., 75, 1217, 1970.

Neugebauer, M., C. T. Russell, and J. V. Olson, Correlated obse tions of electrons and magnetic fields at the earth's bow shock, J. Geophys. Res., 76, 4366, 1971.

Ogilvie, K. W., J. D. Scudder, and M. Sugiura, Electron energy flux in the solar wind, J. Geophys. Res., 76, 8165, 1971.

Ogilvie, K. W., and J. D. Scudder, First results from the six-axis electron spectrometer on ISEE-1, Space Sci. Rev., 23, 123, 1979.

Quest, K. B., Simulations of quasiparallel collisionless shocks, in "Proceedings of the Chapman Conf. on Collisionless Shock Waves in the Heliosphere," Napa Valley, California, 20-24 Feb. 1984.

Reiff, P.H, and D. L. Reasoner, The magnetosheath electron population at lunar distance: general features, J. Geophys. Res., 80, 1232, 1975.

Reasoner, D. L., Observations of low-energy electrons upstream of the earth's bow shock, J. Geophys. Res., 80, 187, 1975.

Scudder, J. D., D.L. Lind, and K. W. Ogilvie, Electron observations in the solar wind and magnetosheath, J. Geophys. Res., 78, 6535, 1973.

Scarf, F. L., R. W. Fredericks, L. A. Frank, and M. Neugebauer, Nonthermal electrons and high-frequency waves in the upstream solar wind 1. Observations, J. Geophys. Res., 76, 5162, 1972.

Thomsen, M. F., H. C. Barr, S. P. Gary, W. C. Feldman, and T. E. Cole, Stability of electron distributions within the earth's bow shock, J. Geophys. Res., 88, 3035, 1983

Thomsen, M. F., J. T. Gosling, S. J. Bame, and M. M. Mellott, Ion and electron heating at collisionless shocks near the critical Mach number, J. Geophys. Res., submitted, 1984.

Tidman, D. A., and N. A. Krall, "Shock Waves in Collisionless Plasmas," Interscience, New York, 1971.

Tokar, R. L., D. A. Gurnett, and W. C. Feldman, Whistler mode turbulence generated by electron beams in earth's bow shock, J. Geophys. Res., 89, 105, 1984.

Winske, D., Microtheory of collisionless shock current layers, in "Proceedings of the Chapman Conf. on Collisionless Shock Waves in the Heliosphere," Napa Valley, California, 20-24 Feb. 1984.

Figure Captions

Figure 1 Measurements of the solar wind flow speed, number density and electron and proton temperatures across both the earth's bow shock at about 0052 UT, 0141 UT and 0155 UT and across an interplanetary shock between 0141 UT and 0155 UT using the Vela 4B plasma analyzer on 26 Feb. 1969. Maximum and minimum values of the electron temperature are given by the two solid line traces and those for the protons are given by the upper and lower endpoints of the vertical lines. Note that the ratio of downstream to upstream proton temperatures across each of the shocks is greater than that for the electrons (from Hundhausen et al., 1970).

Figure 2 Plots of the ratios of downstream to upstream proton and electron temperatures against similar density ratios for 41 interplanetary shocks observed at ISEE 3 between Aug. 1978 and Dec. 1979. The solid lines represent polytrope laws, $T(d/u), = N(d/u)^{\gamma-1}$, for adiabatic compressions in one ($\gamma=3$), two $\gamma=2$) and three ($\gamma=5/3$) dimensions, respectively (from Feldman et al., 1983b).

Figure 3 A scatter plot showing the correlation between upstream and downstream electron and proton temperatures for the same 41 interplanetary shocks in figure 2. The straight line indicates equal ratios (from Feldman et al., 1983b).

Figure 4 Plots of the electron density, temperature and pressure measured aboard ISEE 1 (top) and ISEE 2 (bottom) across the bow shock on 7 Nov. 1977. The wedges above both electron temperature traces indicate the approximate time required for ion thermalization (from Bame et al., 1979).

Figure 5 Cuts through electron velocity distributions measured using Vela 4 during a crossing of the bow shock from the solar wind (1) to the magnetosheath (3) on 5 June 1967 (from Montgomery 1970).

Figure 6 Cuts through ion velocity distributions measured using Vela 4 for the same bow shock crossing as used in figure 5. The numbers in both figures identify the same measurement times. Note that by cut number 2 the ions have slowed but not thermalized whereas the electrons have heated to their maximum downstream temperature (from Montgomery, 1970).

Figure 7 Overlays of cuts through electron velocity distributions aligned parallel (left-hand side) and perpendicular (right-hand side) to $\bar{B}$ measured at ISEE 3 both upstream and downstream of 3 weak interplanetary shocks. Note that all heating is perpendicular to $\bar{B}$ and that both the upstream and downstream cuts through F(v) are Gaussian at low energies (from Feldman et al., 1983c).

Figure 8 Overlays of cuts through electron velocity distributions aligned parallel (left-hand side) and perpendicular (right-hand side) to $\bar{B}$ measured at ISEE 3 both upstream (triangles) and downstream (squares) of a moderately weak interplanetary shock on 4 Oct., 1978. The circles in the right-hand panel gives the upstream velocity distribution transformed assuming the magnetic moment, $\propto v_\perp^2/B$, is conserved (from Feldman et al., 1983c).

Figure 9 Cuts through magnetosheath electron velocity distributions using Vela 4 on 20 June 1967. Note the characteristic flat top at velocities less than about 6000 km/s corresponding to ~100 eV (from Montgomery et al., 1970).

Figure 10 Overlays of cuts through electron velocity distributions measured parallel and perpendicular to $\bar{B}$ downstream of a strong interplanetary shocks at ISEE 3. Note that the heating parallel to $\bar{B}$ is greater than that perpendicular to $\bar{B}$ (from Feldman et al., 1983c).

Figure 11 A scatter plot showing the correlation between the flatness index, $S_{\parallel}$, of parallel cuts through F(v), and the ratio of downstream to upstream density ratios for a set of interplanetary shocks at ISEE 3. $S_{\parallel} = 2$ for a Gaussian and increasing $S_{\parallel}$ yields increasingly flat shapes at low energies as explained in the text (from Feldman et al., 1983c).

Figure 12 A scatter plot showing the correlation between the ratio of downstream to upstream electron temperatures and the flatness index, $S_{\parallel}$, of parallel cuts through F(v), for the same set of interplanetary shocks as used in figure 11.

Figure 13 An overlay of parallel cuts through F(v) measured using ISEE-2 during a crossing of the earth's bow shock from the solar wind (circles) to the magnetosheath (diamonds) on 13 Dec. 1977. Note the formation of a beam at negative electron speeds representing a direction pointed towards the magnetosheath from the solar wind. The beam increases in energy and decreases in amplitude as the penetration toward the magnetosheath increases (from Feldman et al., 1982b).

Figure 14 A schematic picture of the cuts through electron velocity distributions parallel to $\bar{B}$ expected at four different locations ranging from upstream (1) to downstream (4) of the ramp in electrostatic potential, Φ, assuming microinstabilities do not operate. A full explanation is given in the text.

Figure 15 Cuts through electron velocity distributions measured parallel to $\bar{B}$ using ISEE 3 in the deep geomagnetic tail across a slow-mode shock separating the upstream lobe (circles) from the downstream plasma sheet (triangles). The hatched region at negative electron speeds outlines the electrons carrying heat flux from the shock to the upstream lobe in the lobe (circles) and the peak centered at V = +4200 km/s measured within the

shock (squares) shows a beam of electrons accelerated into the downstream plasma sheet.

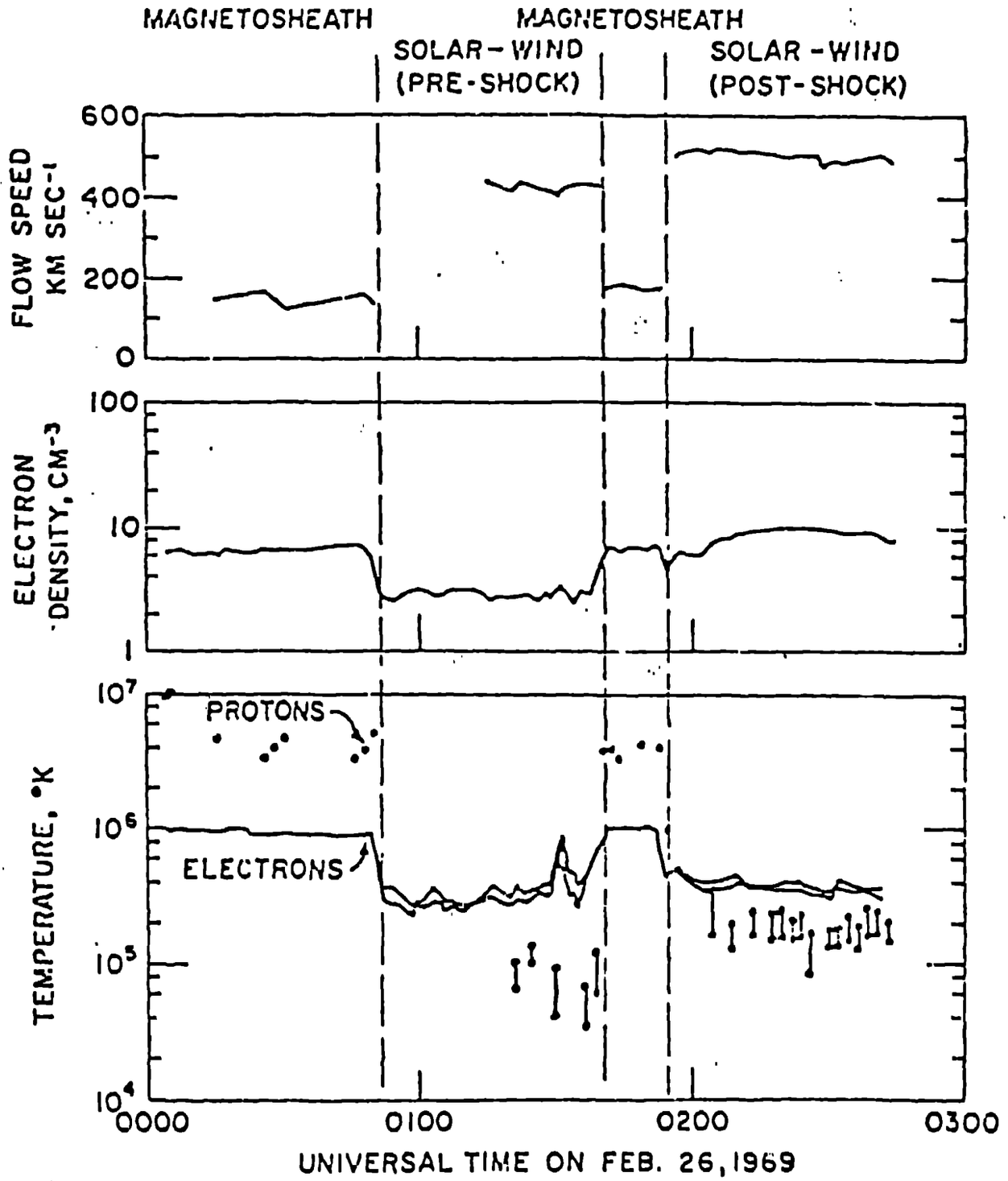
MAGNETOSHEATH
SOLAR-WIND (PRE-SHOCK)
MAGNETOSHEATH
SOLAR-WIND (POST-SHOCK)
FLOW SPEED KM SEC⁻¹
600
400
200
0
ELECTRON DENSITY, CM⁻³
100
10
1
TEMPERATURE, °K
10⁷
10⁶
10⁵
10⁴
PROTONS
ELECTRONS
0000
0100
0200
0300
UNIVERSAL TIME ON FEB. 26, 1969

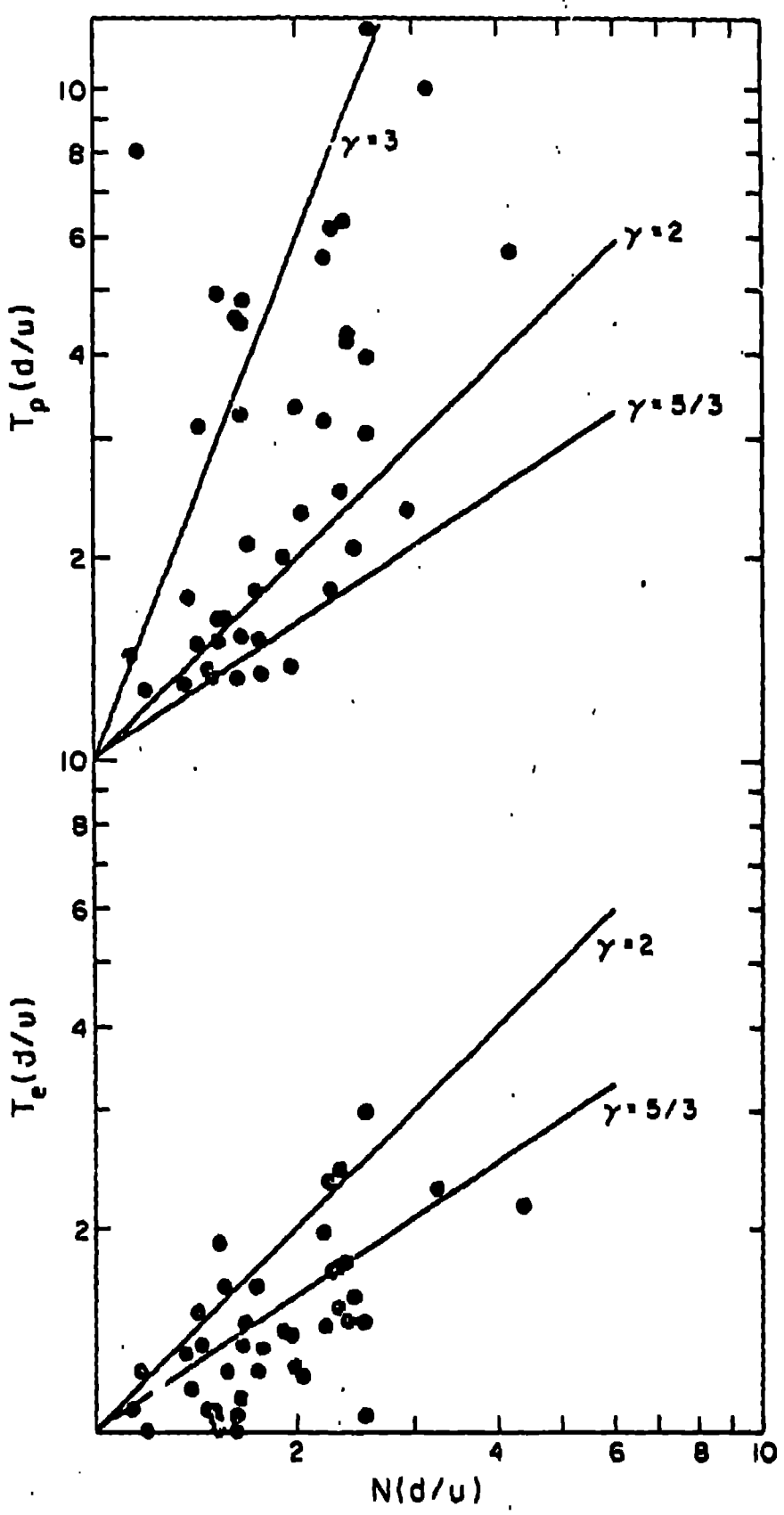
$T_p(d/u)$
$\gamma=3$
$\gamma=2$
$\gamma=5/3$
$T_e(d/u)$
$\gamma=2$
$\gamma=5/3$
$N(d/u)$
2
4
6
8
10

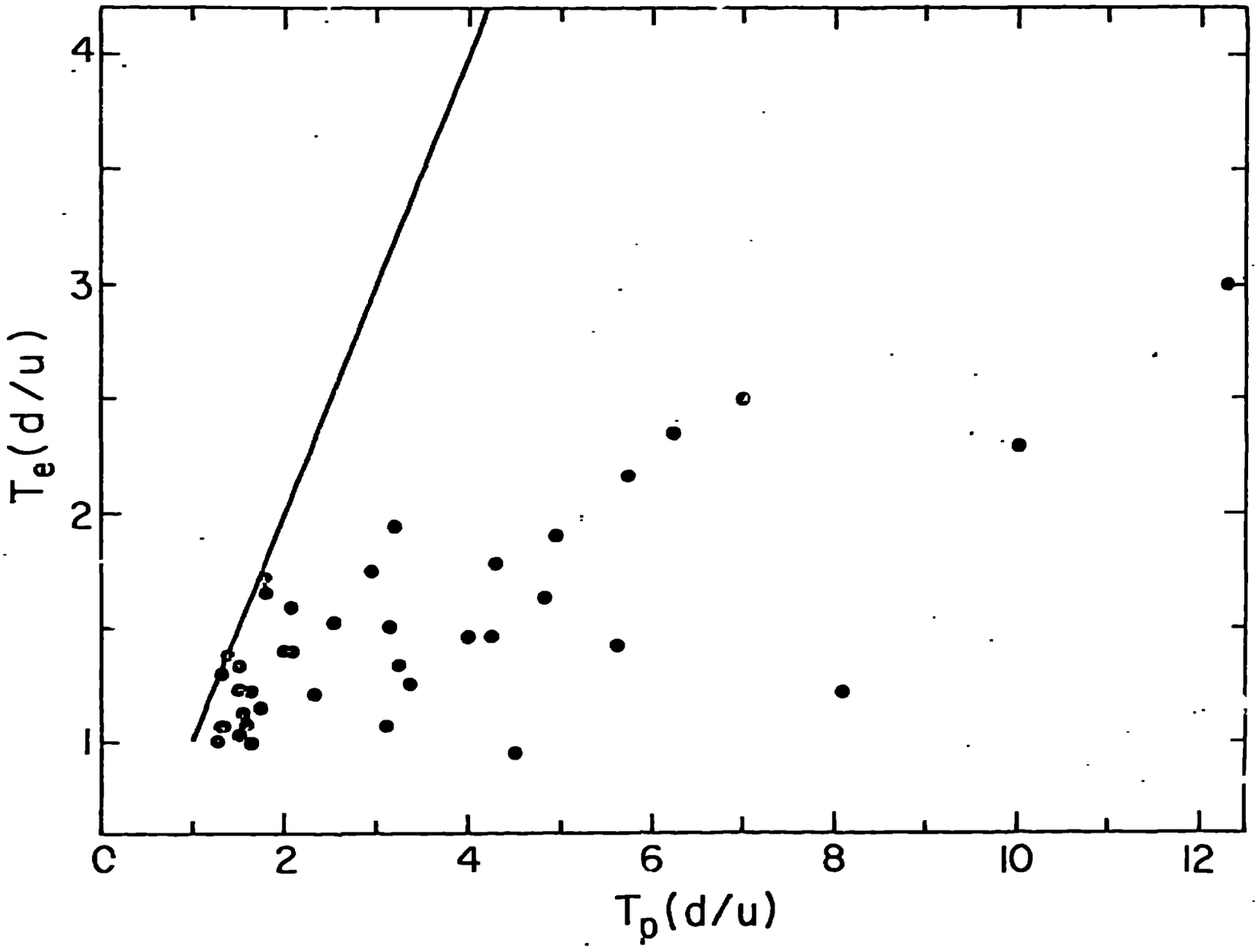

Figure 3

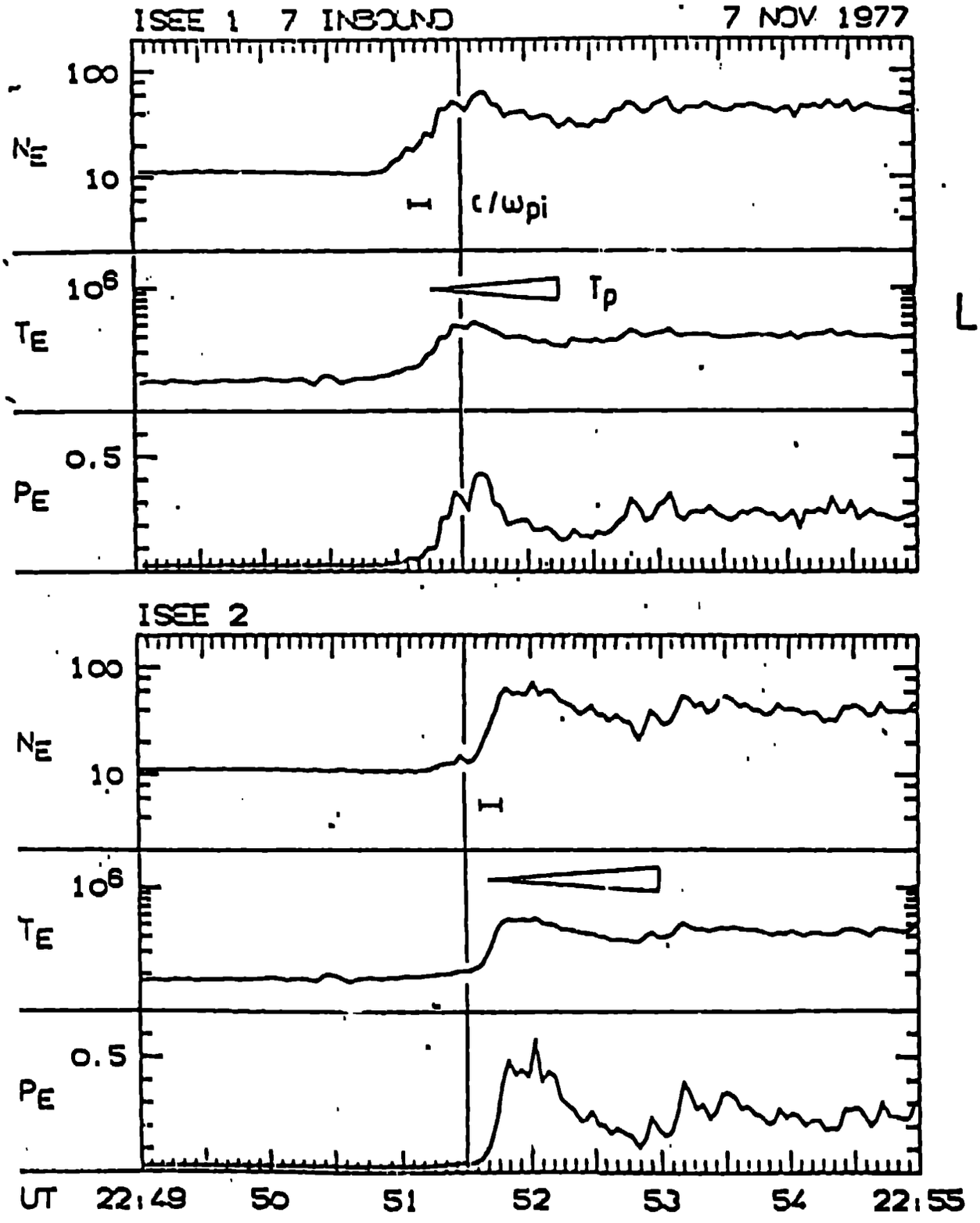
ISEE 1 7 INBOUND
7 NOV 1977
100
N_E
10
c/ω_{pi}
10^6
T_E
T_p
0.5
P_E
ISEE 2
100
N_E
10
10^6
T_E
0.5
P_E
UT 22:49 50 51 52 53 54 22:55
L

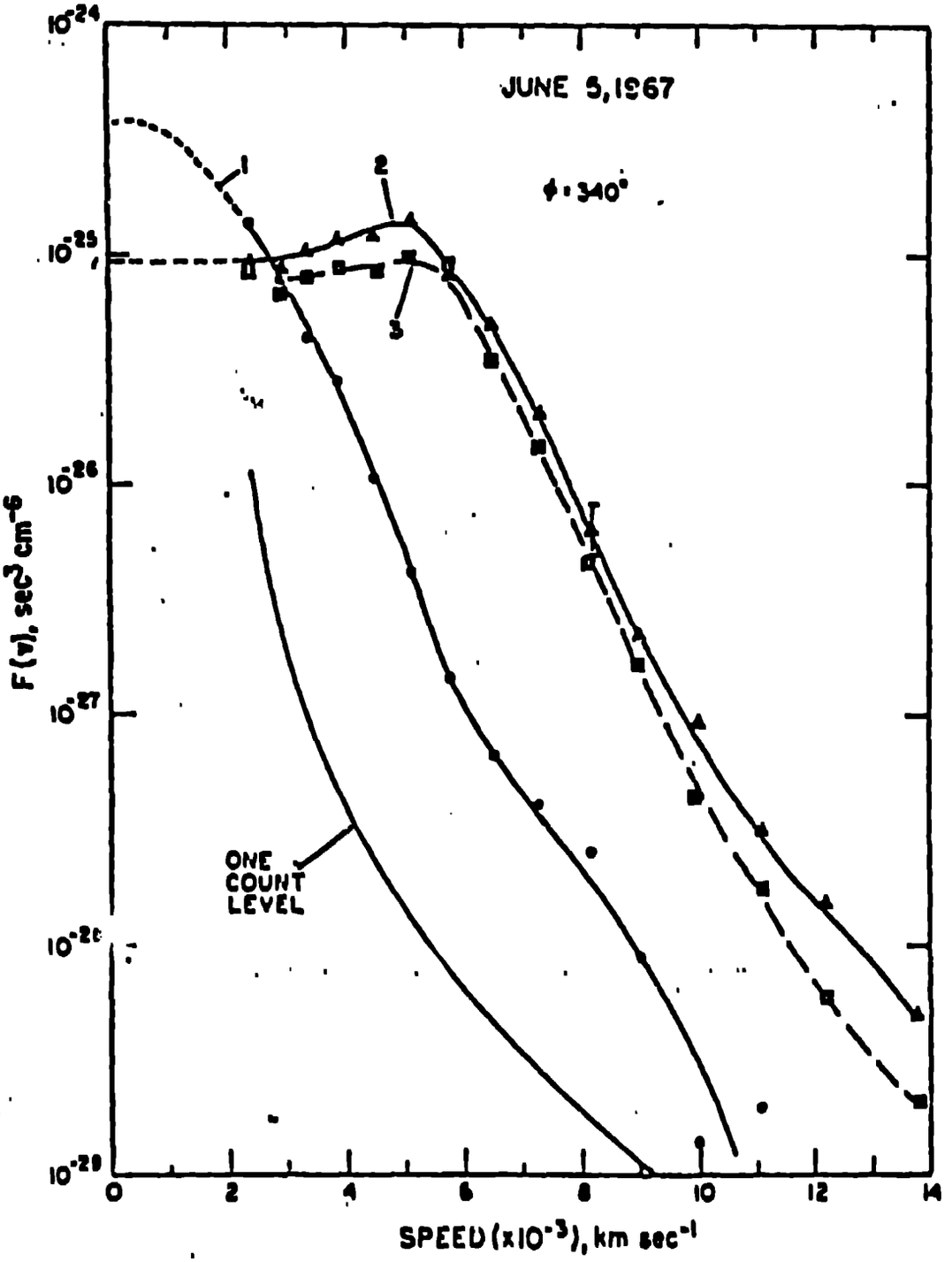
JUNE 5, 1967
φ = 340°
1
2
3
ONE COUNT LEVEL
F(v), sec³ cm⁻⁶
SPEED (x10⁻³), km sec⁻¹
10⁻²⁴
10⁻²⁵
10⁻²⁶
10⁻²⁷
10⁻²⁸
10⁻²⁹
0
2
4
6
8
10
12
14

Fig. 5

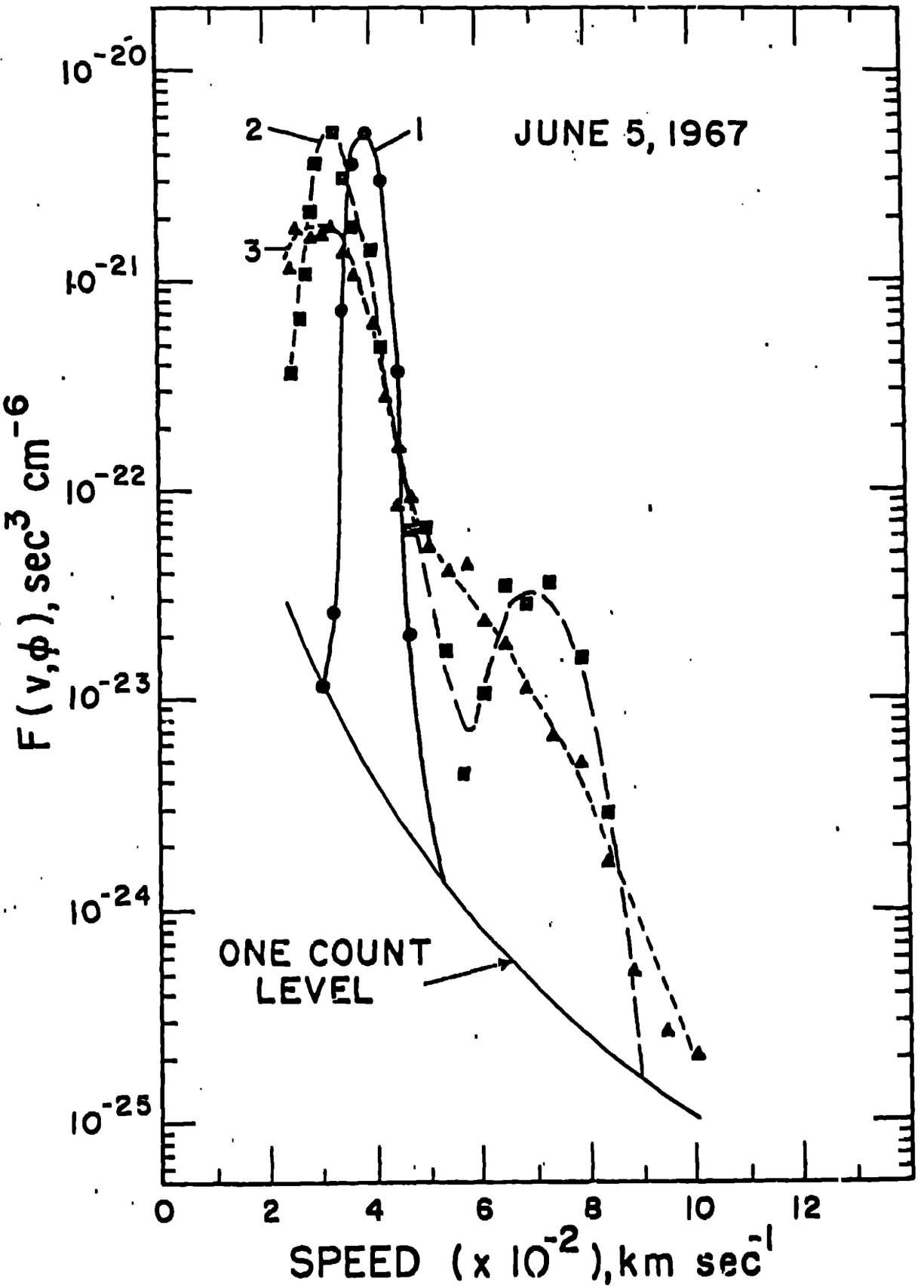
JUNE 5, 1967
1
2
3
ONE COUNT LEVEL
10^{-20}
10^{-21}
10^{-22}
10^{-23}
10^{-24}
10^{-25}
$F(v,\phi)$, $sec^3\ cm^{-6}$
0
2
4
6
8
10
12
SPEED ($\times 10^{-2}$), km sec^{-1}

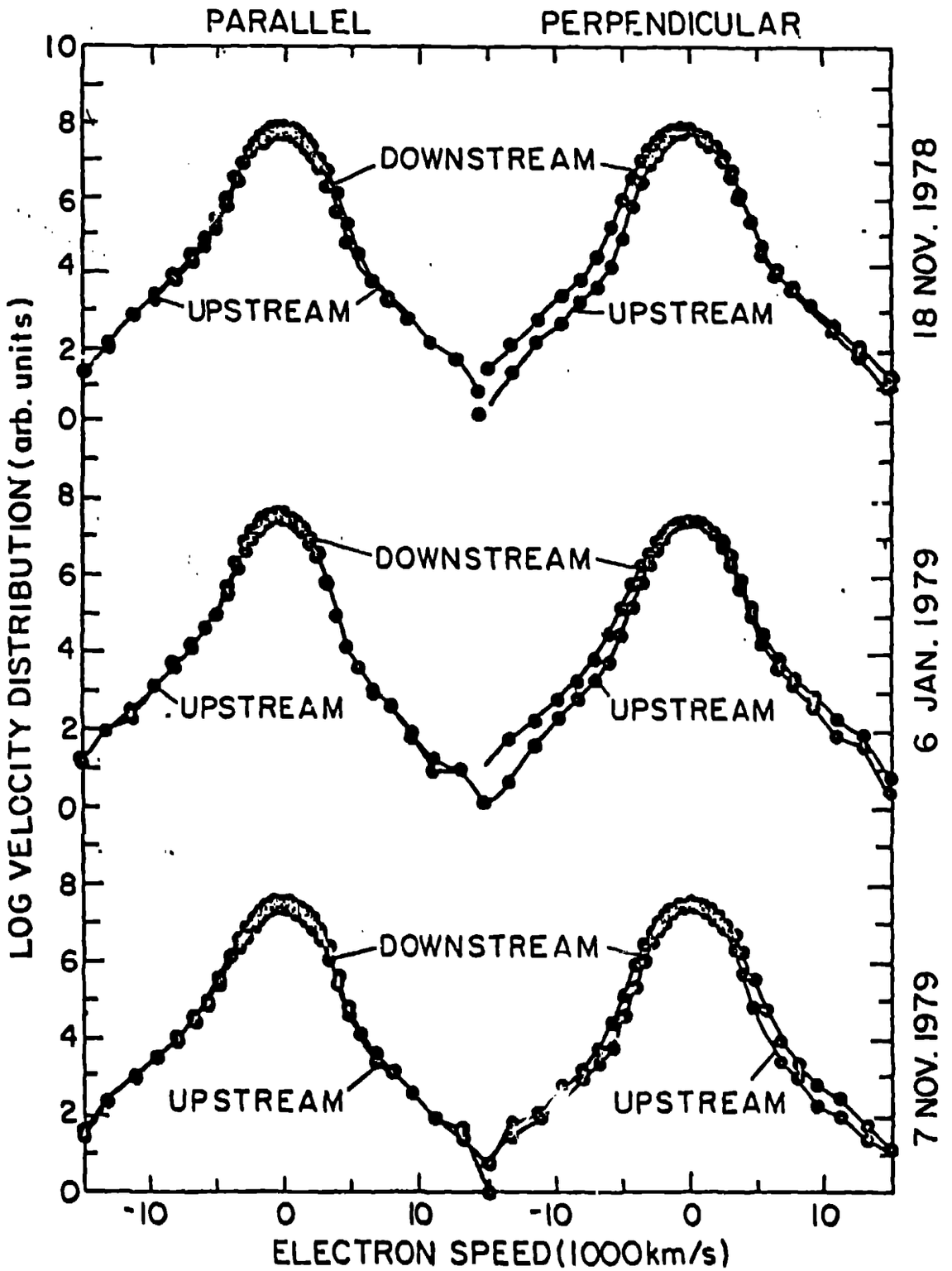
PARALLEL
PERPENDICULAR
LOG VELOCITY DISTRIBUTION (arb. units)
DOWNSTREAM
UPSTREAM
UPSTREAM
18 NOV. 1978
DOWNSTREAM
UPSTREAM
UPSTREAM
6 JAN. 1979
DOWNSTREAM
UPSTREAM
UPSTREAM
7 NOV. 1979
10
8
6
4
2
0
-10
0
10
ELECTRON SPEED (1000km/s)

Fig 7

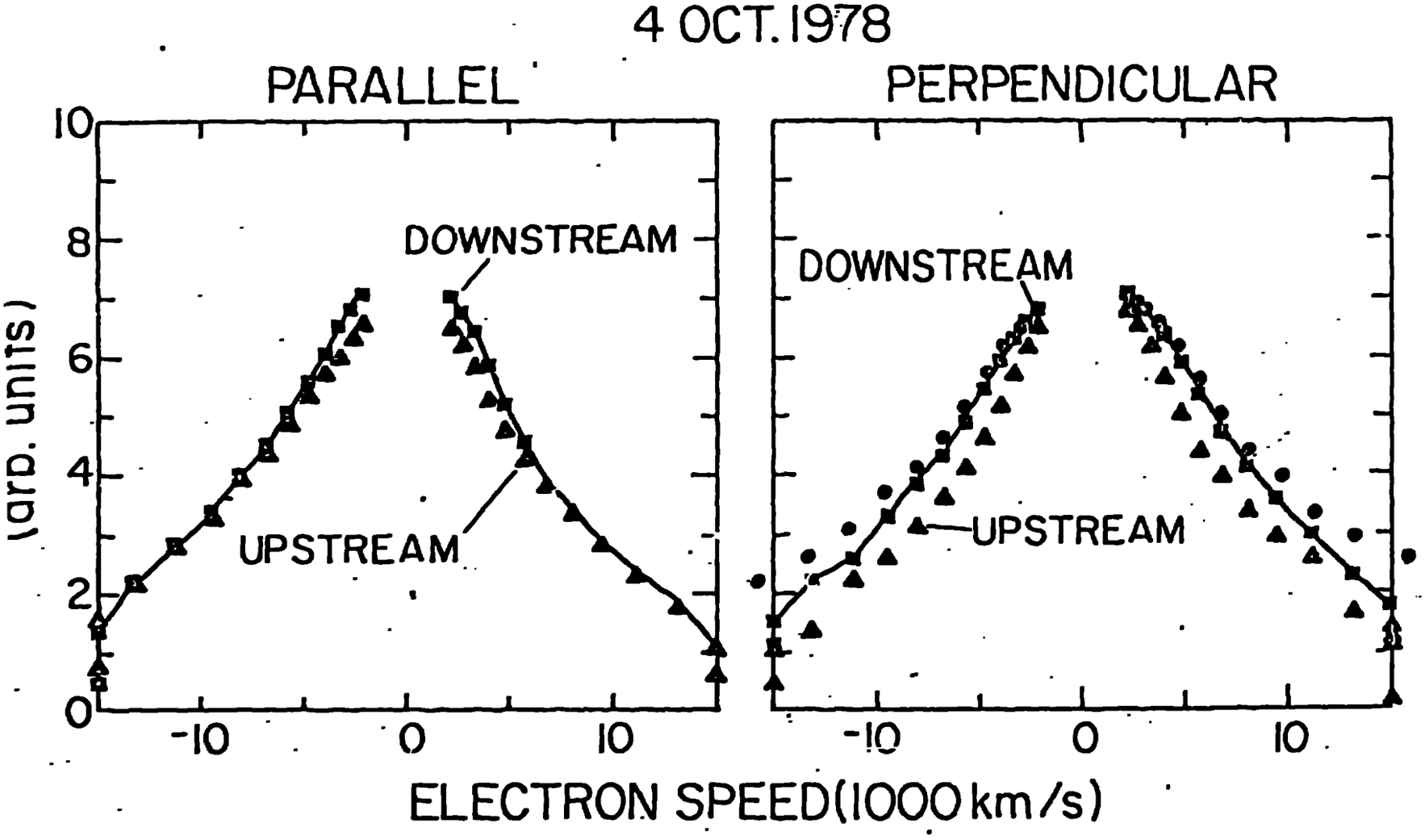
4 OCT. 1978
PARALLEL
PERPENDICULAR
DOWNSTREAM
UPSTREAM
DOWNSTREAM
UPSTREAM
(arb. units)
0
2
4
6
8
10
-10
0
10
-10
0
10
ELECTRON SPEED (1000 km/s)

Fig.

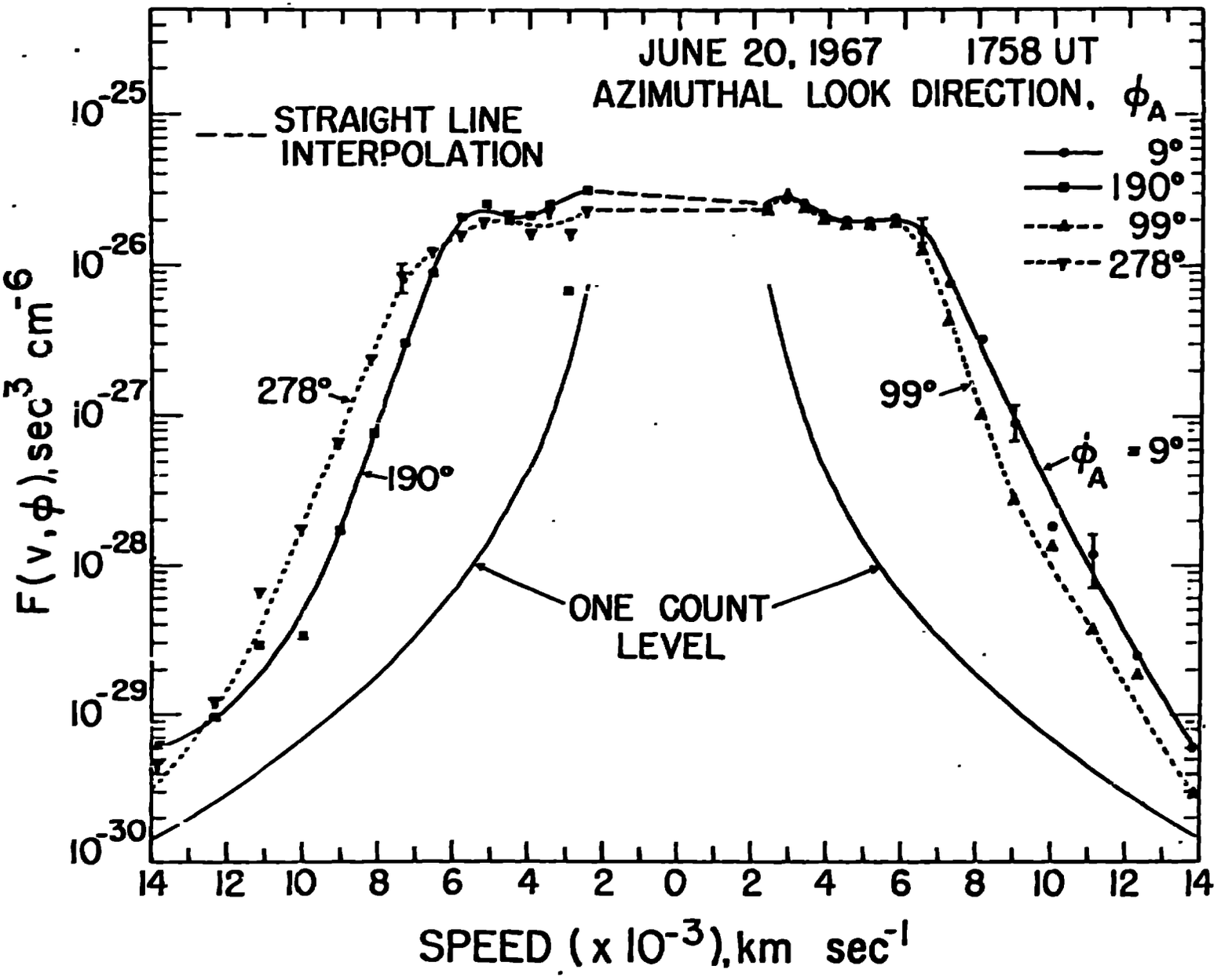
JUNE 20, 1967 1758 UT
AZIMUTHAL LOOK DIRECTION, ϕ_A
STRAIGHT LINE INTERPOLATION
9°
190°
99°
278°
10^{-25}
10^{-26}
10^{-27}
10^{-28}
10^{-29}
10^{-30}
$F(v,\phi)$, sec^3 cm^{-6}
278°
190°
99°
ϕ_A = 9°
ONE COUNT LEVEL
14 12 10 8 6 4 2 0 2 4 6 8 10 12 14
SPEED ($\times 10^{-3}$), km sec^{-1}

Figure 1

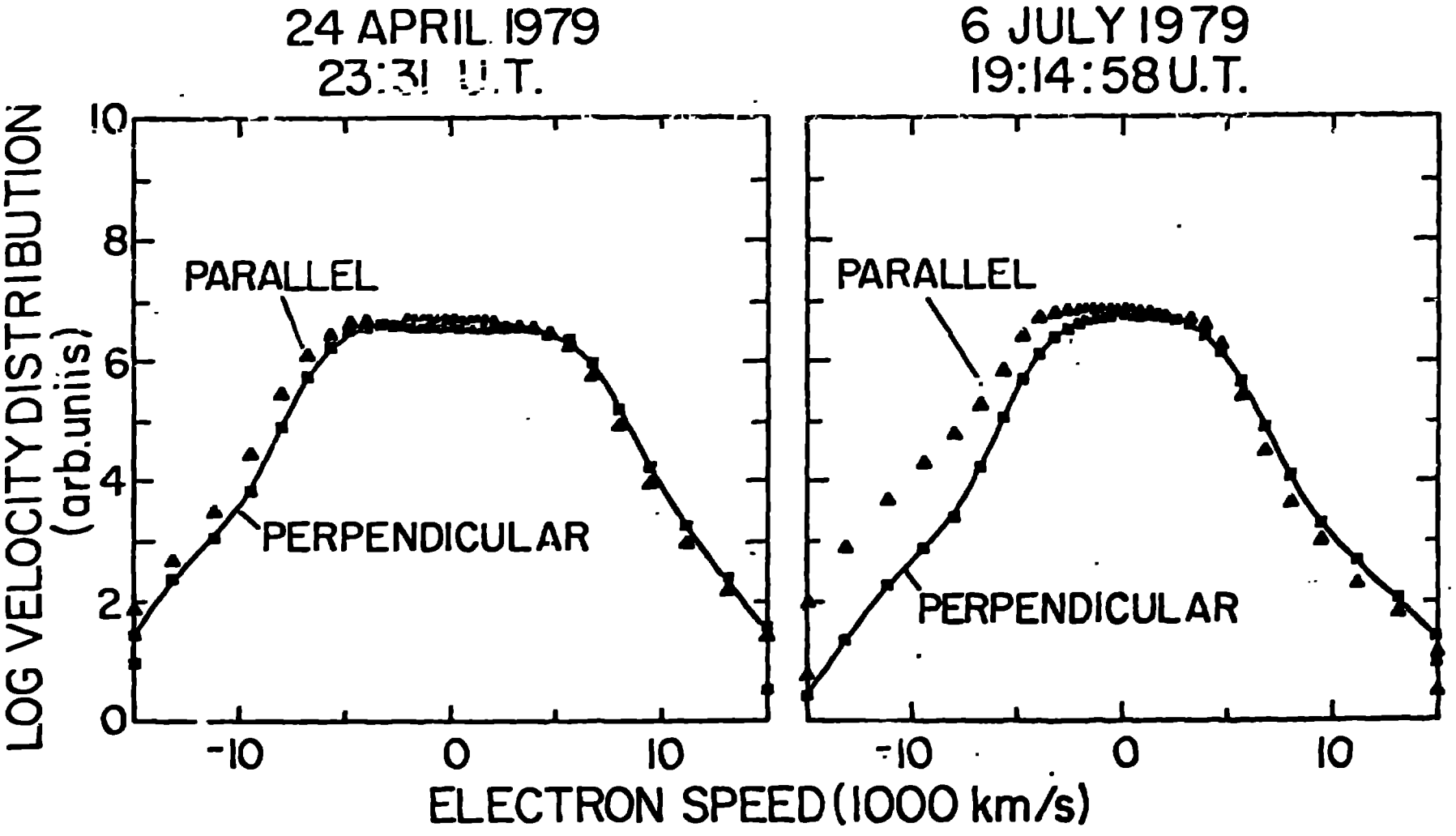
24 APRIL 1979
23:31 U.T.
6 JULY 1979
19:14:58 U.T.
LOG VELOCITY DISTRIBUTION
(arb.units)
PARALLEL
PERPENDICULAR
PARALLEL
PERPENDICULAR
10
8
6
4
2
0
-10
0
10
-10
0
10
ELECTRON SPEED (1000 km/s)

Figure 1

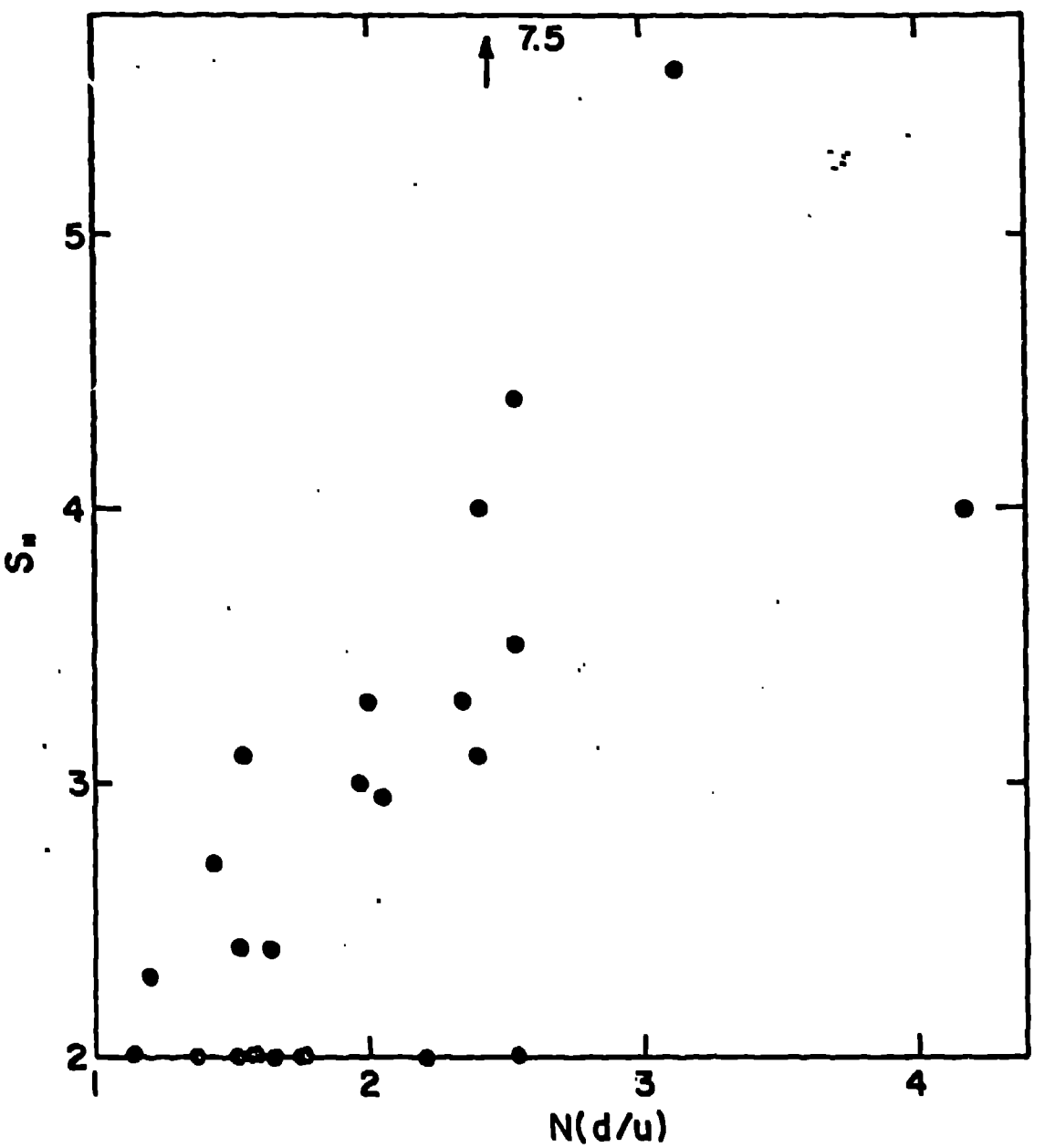
7.5
5
4
3
2
S^{π}
1
2
3
4
N(d/u)

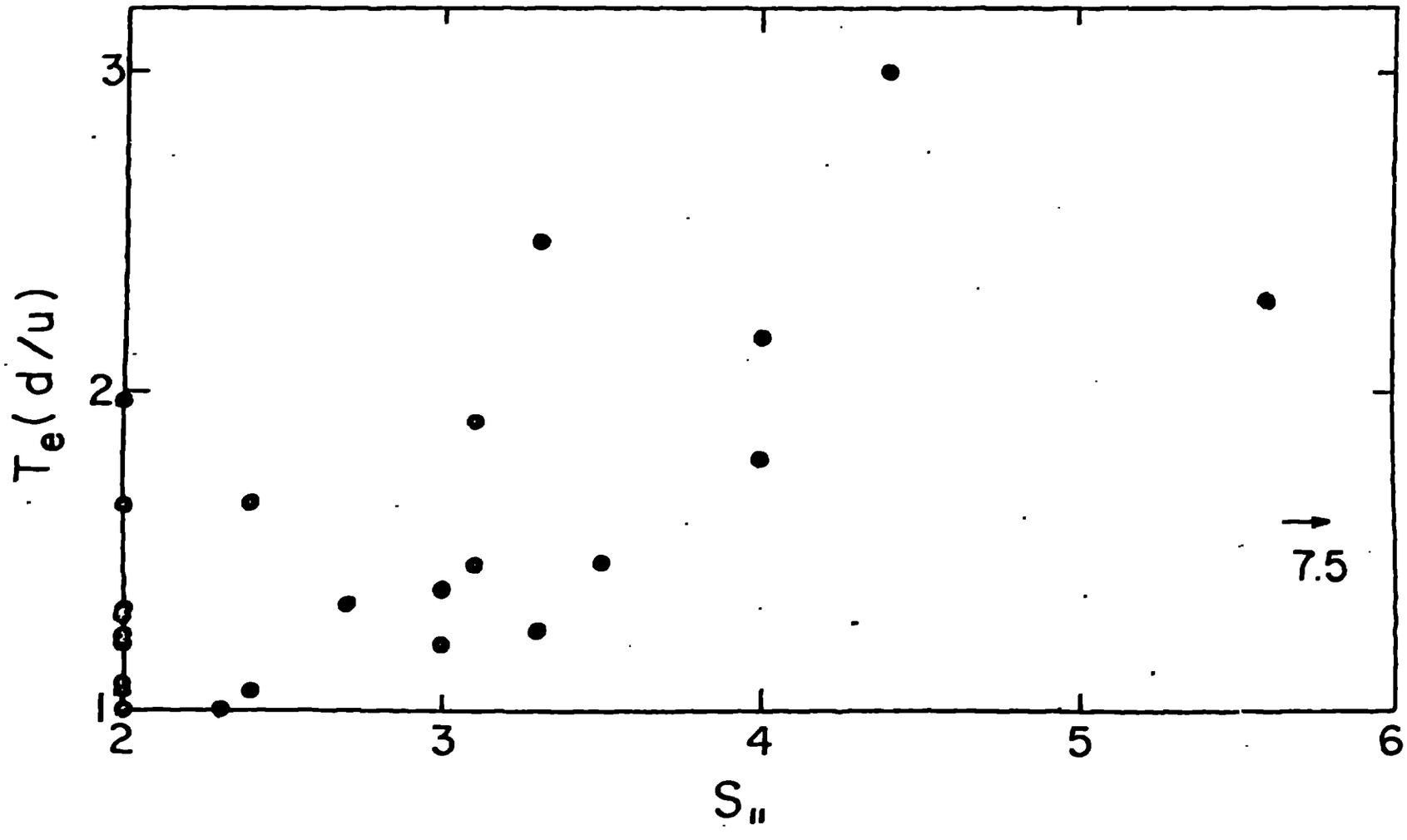
3
2
1
$T_e(d/u)$
2
3
4
5
6
S_{II}
7.5

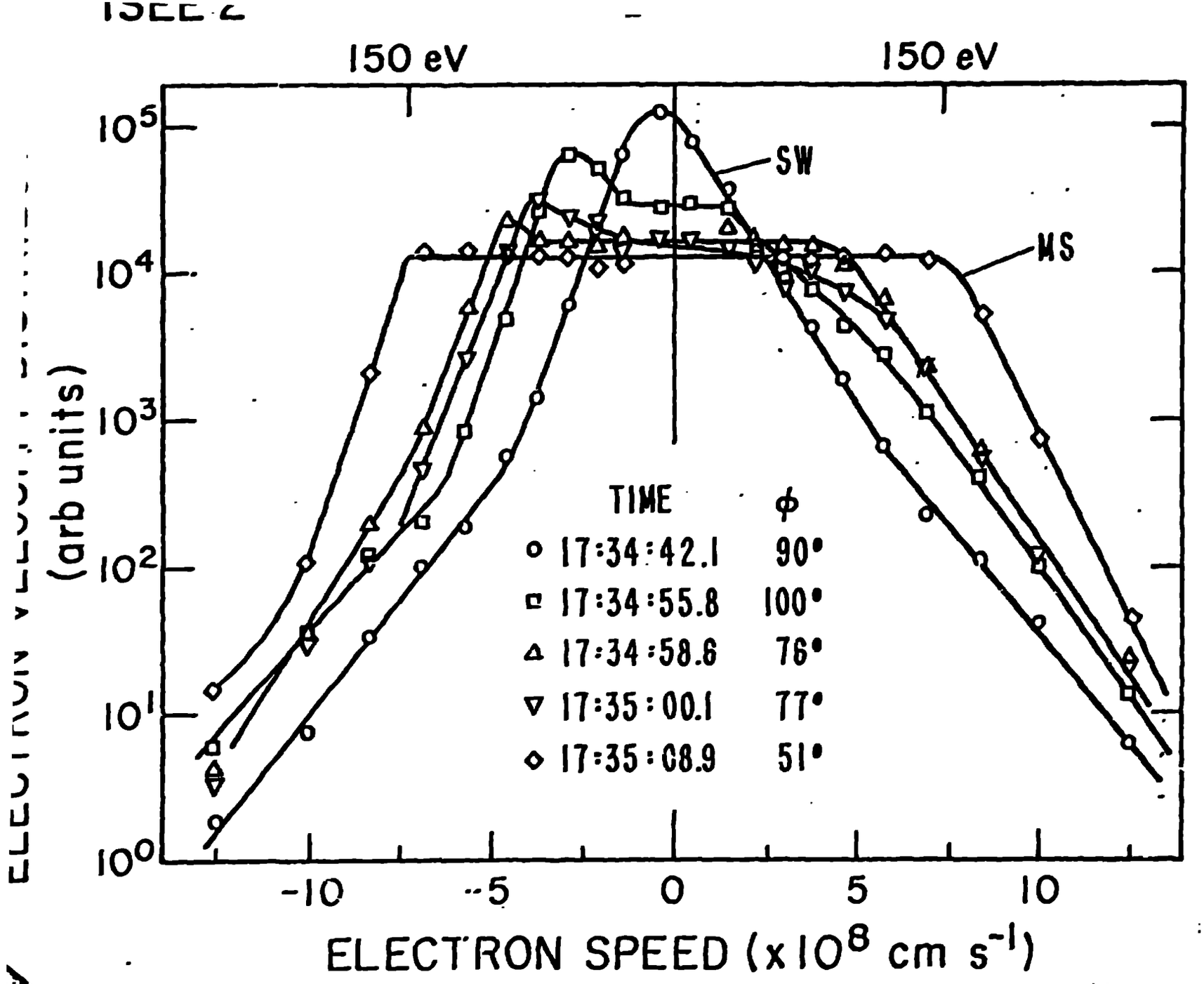
150 eV
150 eV
SW
MS
TIME
φ
17:34:42.1 90°
17:34:55.8 100°
17:34:58.6 76°
17:35:00.1 77°
17:35:08.9 51°
(arb units)
10^5
10^4
10^3
10^2
10^1
10^0
-10
-5
0
5
10
ELECTRON SPEED (x10^8 cm s^-1)

Fig. 2A

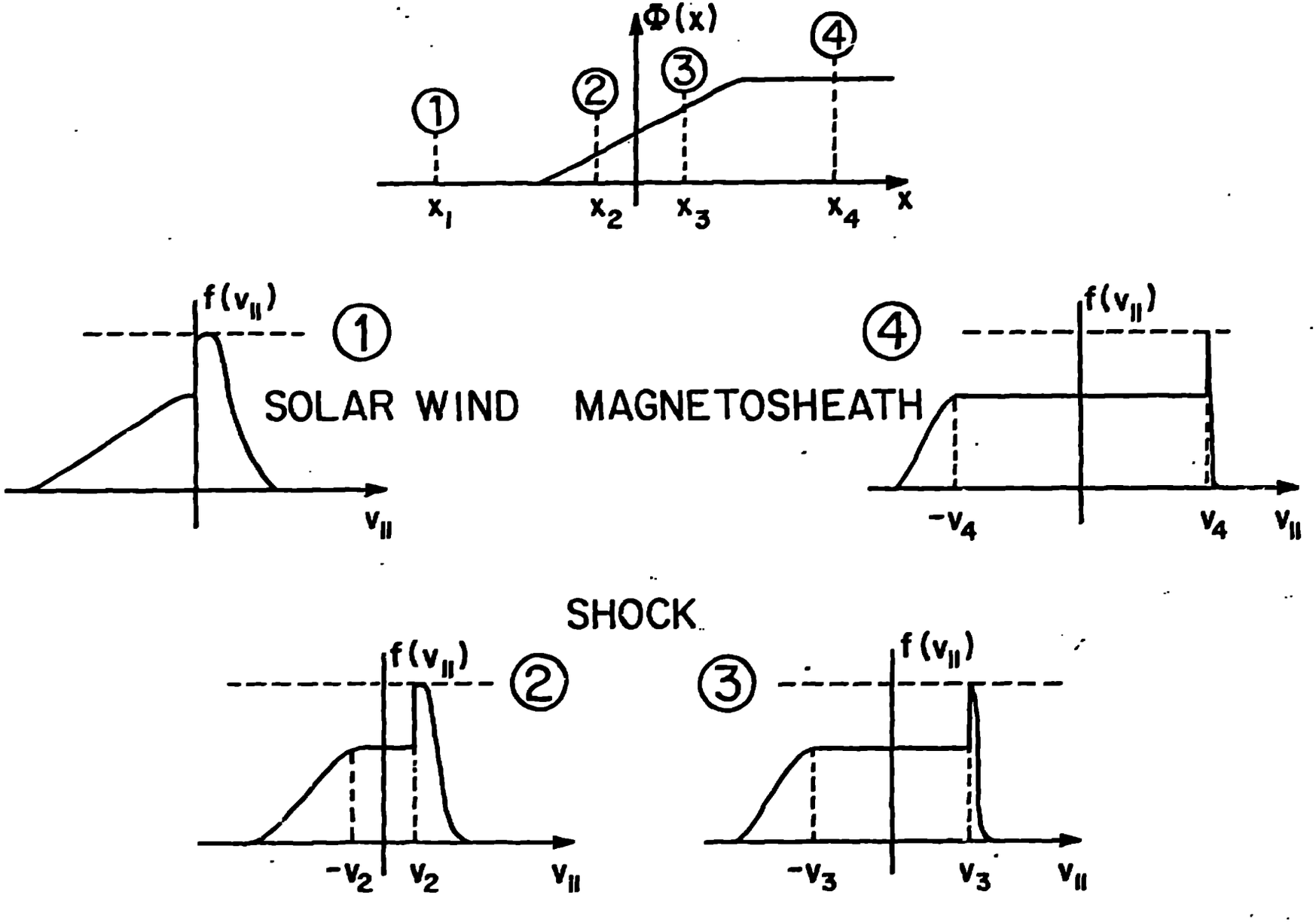
Φ(x)
①
②
③
④
x
x1
x2
x3
x4
f(v||)
v||
SOLAR WIND
MAGNETOSHEATH
-v4
v4
SHOCK
-v2
v2
-v3
v3

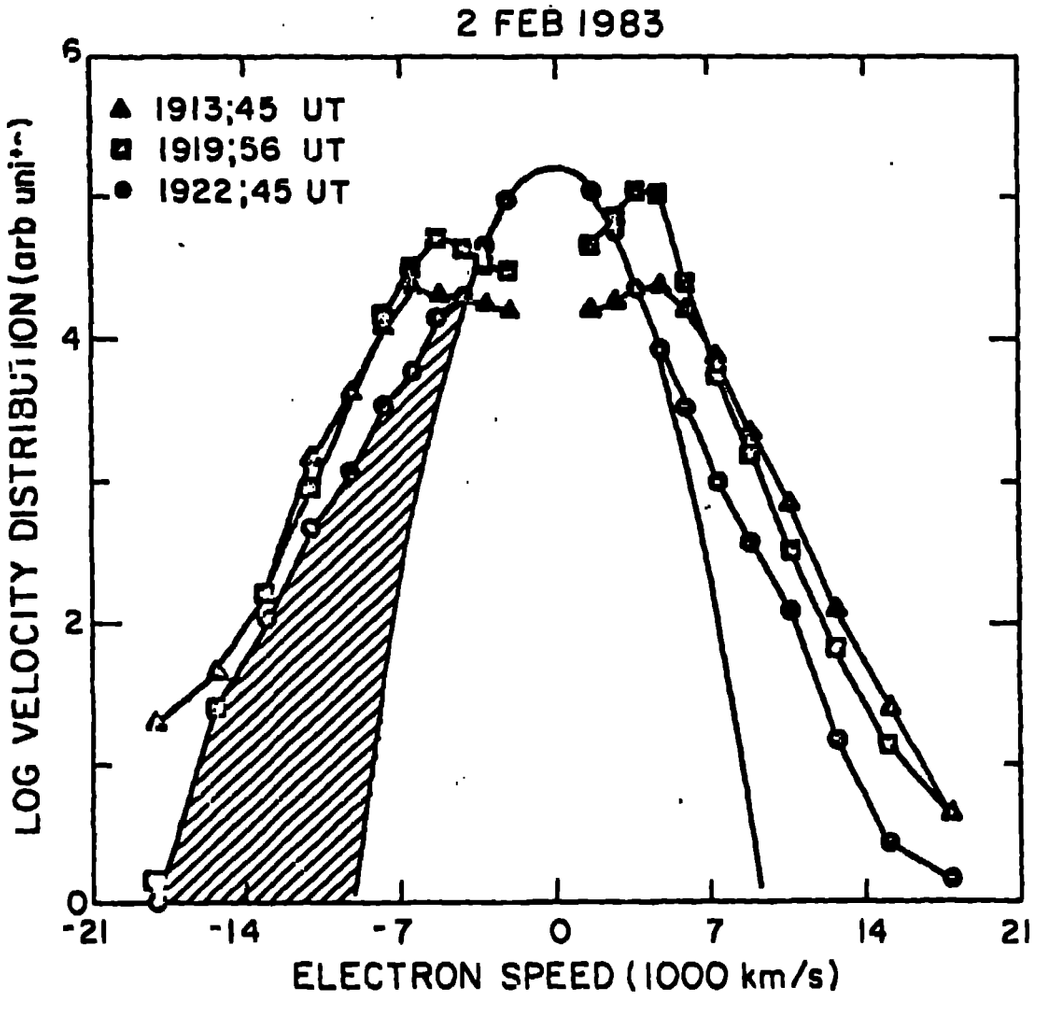
2 FEB 1983
1913;45 UT
1919;56 UT
1922;45 UT
LOG VELOCITY DISTRIBUTION (arb units)
6
4
2
0
-21
-14
-7
0
7
14
21
ELECTRON SPEED (1000 km/s)